


Highly depleted alkali metals in Jupiter’s deep Atmosphere

ANANYO BHATTACHARYA ¹, CHENG LI,¹ SUSHIL K. ATREYA,¹ PAUL G. STEFFES,² STEVEN M. LEVIN,³
SCOTT J. BOLTON,⁴ TRISTAN GUILLOT,⁵ PRANIKA GUPTA,⁶ ANDREW P. INGERSOLL,⁷ JONATHAN I. LUNINE,⁸
GLENN S. ORTON,³ FABIANO A. OYAFUSO,³ J. HUNTER WAITE,^{4,9} AMADEO BELLOTI, AND MICHAEL H. WONG¹⁰

¹University of Michigan, Ann Arbor

²Georgia Institute of Technology

³NASA Jet Propulsion Laboratory

⁴Southwest Research Institute

⁵Universite C’ote d’Azur

⁶University of Michigan

⁷California Institute of Technology

⁸Cornell University

⁹Waite Science LLC

¹⁰University of California, Berkeley

ABSTRACT

Water and ammonia vapors are known to be the major sources of spectral absorption at pressure levels observed by the microwave radiometer (MWR) on Juno. However, the brightness temperatures and limb darkening observed by the MWR at its longest wavelength channel of 50 cm (600 MHz) in the first 9 perijove passes indicate the existence of an additional source of opacity in the deep atmosphere of Jupiter (pressures beyond 100 bar). The absorption properties of ammonia and water vapor, and their relative abundances in Jupiter’s atmosphere do not provide sufficient opacity in the deep atmosphere to explain the 600 MHz channel observation. Here we show that free electrons due to the ionization of alkali metals, i.e. sodium, and potassium, with sub-solar metallicity, $[M/H]$ (log based 10 relative concentration to solar) in the range of $[M/H] = -2$ to $[M/H] = -5$ can provide the missing source of opacity in the deep atmosphere. If the alkali metals are not the source of additional opacity in the MWR data, then their metallicity at 1000 bars can only be even lower. This upper bound of -2 on the metallicity of the alkali metals contrasts with the other heavy elements – C, N, S, Ar, Kr, and Xe – which are all enriched relative to their solar abundances having a metallicity of approximately +0.5.

Keywords: Solar System (1528) – Chemical abundances(224) – Jupiter(873) – Extrasolar gaseous giant planets(509)

1. INTRODUCTION

The alkali metals sodium and potassium have been previously detected in the atmospheres of hot Jupiters and a super-Neptune together with lithium [Chen et al. (2018)] in the latter. The detections show a large range of abundances from highly substellar to super-stellar values [Welbanks et al. (2019), Demory et al. (2011)]. Alkali metal abundances are important in understanding the formation of hot Jupiters and represent a bridge between the refractory and volatile elements, which in molecular form seed the growth of planets. Obtaining the abundance of alkali metals in Jupiter can potentially serve as a first constraint on the ratio of rocky to icy material in the interior of the solar system’s largest planet when combined with the elemental and molecular abundances provided by the Galileo Probe Mass Spectrometer (GPMS) [Atreya et al. (1999), Wong et al. (2004), Atreya et al. (2019)] and Juno constraints on water [Li et al. (2020)]. Here we derive observationally based abundances of alkali metals in

Jupiter’s atmosphere to determine whether they are enriched relative to solar like the other heavy elements or depleted.

To obtain these abundances requires knowing the deep structure of Jupiter’s atmosphere. The shallower part of Jupiter’s atmosphere has been previously investigated at microwave frequencies by the Very Large Array (VLA) telescope [de Pater & Dunn (2003), de Pater et al. (2019)]. VLA probes Jupiter at frequencies in the range of 74 MHz to 50 GHz [de Pater et al. (2019)]. However, confusion from Jupiter’s powerful synchrotron radiation does not allow VLA to observe Jupiter’s atmosphere below 5 GHz [de Pater & Dunn (2003)], limiting its reach to less than 5 bars, leaving the deep atmosphere of Jupiter inaccessible from microwave and radio frequency observatories from Earth. The orbit of Juno and the spin of the spacecraft allow the spacecraft to make observations at low frequencies, i.e. 0.6 GHz and 1.2 GHz, by avoiding the energetic electron belts around Jupiter from its field of view. Access to greater depths allows for the investigation of bulk elemental abundances of N and O in Jupiter [Janssen et al. (2017), Bolton et al. (2017), Steffes et al. (2017)].

The Microwave Radiometer (MWR) instrument onboard the Juno orbiter is a passive radiometer that is designed to measure the internal heat emitted by Jupiter’s atmosphere at six different frequencies ranging from 0.6 GHz to 22 GHz [Janssen et al. (2017)]. The brightness temperature measured by MWR at these frequencies sounds different levels of Jupiter’s atmosphere corresponding to pressures from 0.3 bar to 250 bar [Janssen et al. (2017)]. In addition, the highly inclined polar orbit and rotation of the Juno spacecraft aided in the high spatial resolution necessary for probing Jupiter’s atmosphere at various latitudes [Bolton et al. (2017)].

Previous analysis of the MWR data at the 0.6 GHz found an unanticipated limb-darkening signal, which cannot be explained by nominal absorbers such as ammonia and water [Li et al. (2020)]. Based on investigation of thermodynamic models of Jupiter’s deep atmosphere between 50 bar and 1 kbar [Fegley Jr & Lodders (1994), Weidenschilling & Lewis (1973)] we conjecture that the free electrons from thermally ionized alkali metals may provide the missing opacity. Alkali metals are expected to undergo condensation to form clouds in the deep atmosphere [Visscher et al. (2006), Morley et al. (2012)]. Na₂S and KCl are the first chemical species to condense in the above pressure range and thereby act as a sink for atomic sodium and potassium [Fegley Jr & Lodders (1994)]. Furthermore, high-temperature environments cause alkali metals to undergo ionization due to their low ionization energies [Bagenal et al. (2007)]. Density and temperature play a role in governing the electron densities according to the Saha ionization equation (Eq. 2). Electrons generated from alkali metal ionization act as a source of absorption at microwave frequencies that could affect the brightness temperatures at the 0.6 GHz frequency channel. Therefore, the objective of this study is to determine the alkali metal abundance in the deep atmosphere of Jupiter.

To facilitate comparison of our results on alkali metals with those of the extrasolar planets we express the abundances of non- hydrogen and helium elements using astronomical terminology, e.g., metallicity. The metallicity ($[M/H]$) of an element is the logarithm of the ratio of elemental abundance in a system to the stellar (or solar, for the solar system) elemental abundance. Generally, the metallicity of a star is defined in terms of the ratio of the number of Fe atoms to the number of hydrogen atoms. Here we define the metallicity in terms of alkali metal abundance in Jupiter to that of Sun e.g. for potassium, $[K/H] = \log_{10}(N_K/N_H)_{Jupiter} - \log_{10}(N_K/N_H)_{Sun}$. For the giant planets, iron and silicon is not measurable, emphasizing the importance of proxy indicators such as the alkali metals along with other elements measured by Galileo probe.

2. METHODS

Brightness temperatures from 9 perijoves i.e. PJ 1,3-9, 12 have been taken into consideration for this article. Variations in brightness temperatures have been observed across the planetocentric latitudes from pole-to-pole at 0.6 and 1.2 GHz channels. These variations can be attributed to various sources of origin from the atmosphere and space environment. The most important sources of the observed variability are (i) changes in atmospheric structure and composition, (ii) Jupiter’s synchrotron radiation in the microwave band, and (iii) variation in acceleration due to gravity due to the non-spherical shape of Jupiter. The latter sources, i.e. synchrotron and gravity need to be taken into account for proper interpretation of MWR observations. It will aid in investigating the true variability in

Jupiter’s deep atmosphere.

The contribution of Jupiter’s gravity can be corrected by taking into account the non-spherical shape of Jupiter. Brightness temperatures are corrected using a gravity correction factor defined as the ratio of theoretical T_b at a given latitude to that at the equator of Jupiter taking into consideration the acceleration due to gravity at the latitude. Thereby, it transforms the Juno observations at each latitude for equatorial gravity, which effectively removes variation in T_b due to changes in Jupiter’s gravity from the equator to the poles.

Energetic electrons in Jupiter’s space environment contribute to the synchrotron radiation [de Pater & Dunn (2003), Levin et al. (2001), Santos-Costa et al. (2017)]. The signature of the emission is observed in MWR data across all the perijoves which leads to anomalous changes in T_b . Data at extremely high latitudes are polluted by synchrotron emission and thus, remain of no use for investigating Jupiter’s deep atmosphere. Therefore, we only consider the MWR data between -60 to 60 deg. latitude. The correction for synchrotron and other sources of anomalous T_b is done by filtering the data at 0.6 and 1.2 GHz for each perijove. The process is carried out by sorting the deviations of T_b from the least value of T_b in a group and removing the values greater than a filter cutoff temperature of the order of 2 K.

3. RESULTS

3.1. Sources of Microwave Opacity

The weighting function of Jupiter’s atmospheric absorption and emission at a given microwave frequency determines the contribution of each region in the atmosphere to the observed brightness temperature at the given frequency. The peak structure of the weighting function gives the range of pressure levels corresponding to the measurements. The weighting function can be expressed as a function of microwave opacity of the atmosphere (1). Here, T_b is the brightness temperature, $W(p)$ is the weighting function as a function of pressure, and $T(p)$ is the physical temperature profile of the atmosphere.

$$T_b = \int_{-\infty}^{\infty} W(p)T(p)d\ln P \quad (1)$$

Fig. 1 shows the relative weighting functions, i.e. weighting function divided by the maximum value of the function, at 0.6 GHz and 1.2 GHz with and without alkali metals. In the absence of alkali metals, the relative weighting functions peak at 100 bar and 30 bar, respectively [Janssen et al. (2017)]. At 0.6 GHz, the relative weighting function extends to the deeper atmosphere below the 100 bar level, and therefore, the T_b derived using this channel is sensitive to the sources of microwave opacity present in the deep atmosphere at p greater than 100 bar. The relative weighting function at 0.6 GHz channel shows a broad shape with a second maxima at kbar pressure levels which is attributed to the increase in mass absorption coefficients of water vapor with pressure. The mass absorption coefficient of ammonia decreases after a maximum near 1000 bar and eventually water vapor dominates the opacity in the deep atmosphere. Moreover, the inclusion of free electrons as sources of opacity due to alkali metal ionization causes a decrease in the value of the relative weighting function at 0.6 GHz around 100 bar, and a global maximum in the relative weighting function emerges at ~ 1 kbar pressure (magenta line). The shift of the global maximum can be attributed to the increase in opacity from free electrons with pressure as the ionization fraction of alkali metals increases with temperature under thermal equilibrium conditions [Saha (1920)] (described later in this section). Inclusion of lower amounts of alkali metals ($[M/H] = -5$) will lead to a peak at deeper levels (Fig. 1). However as the metallicity is increased to solar, the maximum drifts towards lower pressures around 1 kbar level. This could be attributed to the fact that higher abundance of alkali metals can produce higher amount of electrons at relatively lower pressures (magenta line), whereas low abundance of alkali metals in Jupiter would need to reach higher pressure (> 1 kbar) to produce equivalent opacity (blue line). Thereby the abundance of alkali metals directly affects the shape of weighting function.

The main sources of microwave opacity at 0.6 GHz and 1.2 GHz are ammonia, water vapor, free electrons, and collision-induced absorption by hydrogen and helium. Hydrogen-hydrogen and hydrogen-helium collisions are the dominant sources of collision-induced absorption processes in Jupiter. Their magnitude is well constrained due to the invariance of hydrogen and helium abundances in Jupiter’s deep atmosphere. The microwave absorption behavior of

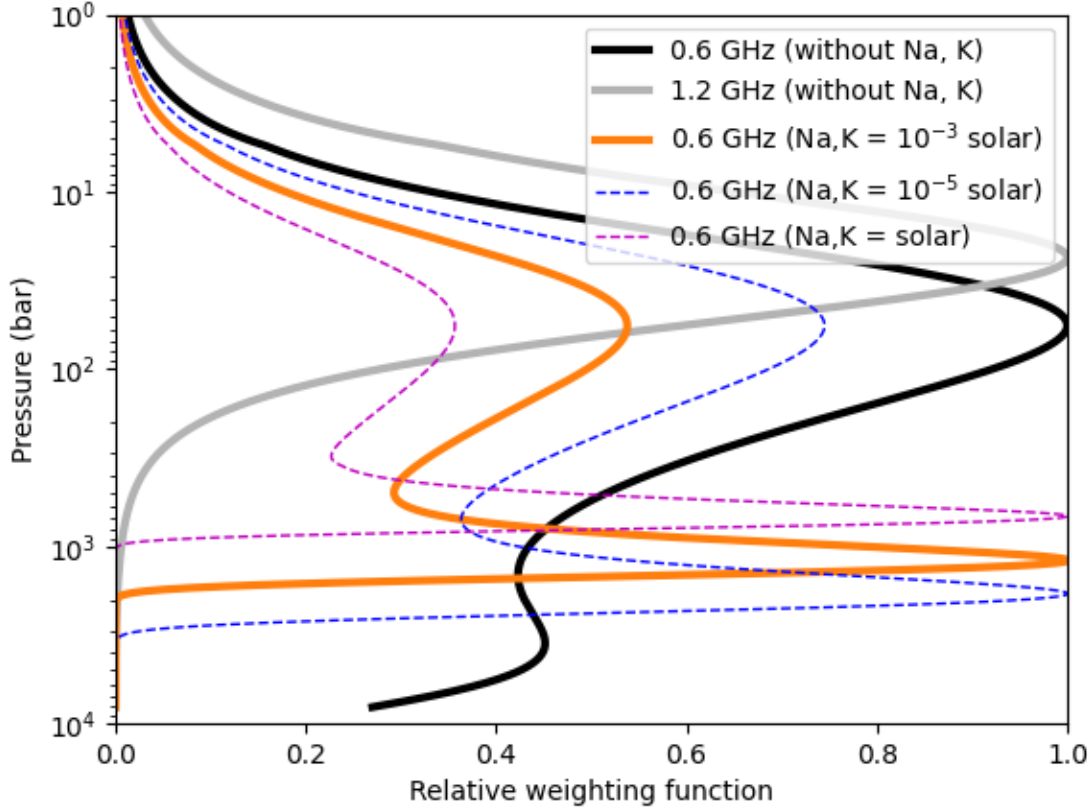


Figure 1. Relative weighting functions at 0.6 GHz (black) and 1.2 GHz (gray) for a Jupiter adiabat considering the Hanley model [Hanley et al. (2009)] for NH_3 absorption. The functions peak at 100 bar and 30 bar at 0.6 GHz and 1.2 GHz respectively without the inclusion of alkali metals. The inclusion of alkali metals (orange, magenta and blue) decreases the relative weighting function at ~ 100 bar and produces a second peak that is observed at ~ 1 kbar pressure due to the opacity contributed by free electrons from alkali metal ionization. As the metallicity of alkali metals increase, the global maximum of weighting function shifts towards lower pressure.

water and ammonia vapor has been investigated by laboratory experiments that show the pressure and temperature dependence of mass absorption coefficients [Devaraj et al. (2014), Karpowicz & Steffes (2011), Bellotti et al. (2016)]. In addition, hydrogen, methane, and water vapor contribute to line broadening in the ammonia vapor absorption. The models based on laboratory experiments show significant divergent behavior when extrapolated to pressures greater than 50 bar and 550 K [Bellotti et al. (2016)]. In order to obtain a robust estimate of the range of absorption coefficients at higher temperatures, we test a grid model describing a power scaling relationship with temperature based on the Hanley et al. (2009) model of ammonia absorption. For water vapor absorption at microwave frequencies, the laboratory models show divergence by orders of magnitude. However, recent laboratory measurements [Steffes et al. (2023)] at high pressure show that water vapor absorption can be explained by the Bellotti et al. (2016) model. Therefore, Bellotti et al. (2016) model is chosen to compute the water vapor opacity which incorporates water opacity measurements at high temperatures above 500 K.

Free electrons in the atmosphere can act as a source of opacity at microwave wavelengths through the process of free-free absorption in which electrons absorb photons during collisions with other ions and electrons. Electrons can be generated by the ionization of various elemental and molecular species in the atmosphere. Due to their low ionization energies, alkali metals i.e. Na, K are expected to be the major sources of free electrons in the atmosphere [Heays et al. (2017)]. In Jupiter’s atmosphere, the pressure and temperatures corresponding to the transition between the alkali metals and their compounds are calculated using an equilibrium cloud condensation model (ECCM) [Atreya

et al. (1999), Weidenschilling & Lewis (1973)] for Jupiter’s adiabat with saturation vapor pressures of Na_2S and KCl [Visser et al. (2006), Morley et al. (2012)]. The condensation of alkali metals at solar abundance [Figure 2] takes place at 352 bar for KCl and 796 bar for Na_2S , with corresponding temperatures of 967 K and 1234 K, respectively, assuming thermodynamic equilibrium. The condensation of Na_2S at deeper levels, and a higher solar abundance of Na compared to K [Asplund et al. (2009)] will cause Na_2S clouds to be significantly more massive than KCl clouds. Thermochemical equilibrium models indicate formation of metal hydrides and hydroxides in gas phase, however they are much lower in abundance [Fegley Jr & Lodders (1994)] as compared to the condensates, thereby they will not act as the primary sink of alkali metals in Jupiter. Condensation of the alkali metal compounds occurs when the partial pressure of a compound exceeds its saturation vapor pressure. If condensation occurs, it causes depletion in the alkali metal abundances at altitudes above the condensation level.

Jupiter Condensation Curves

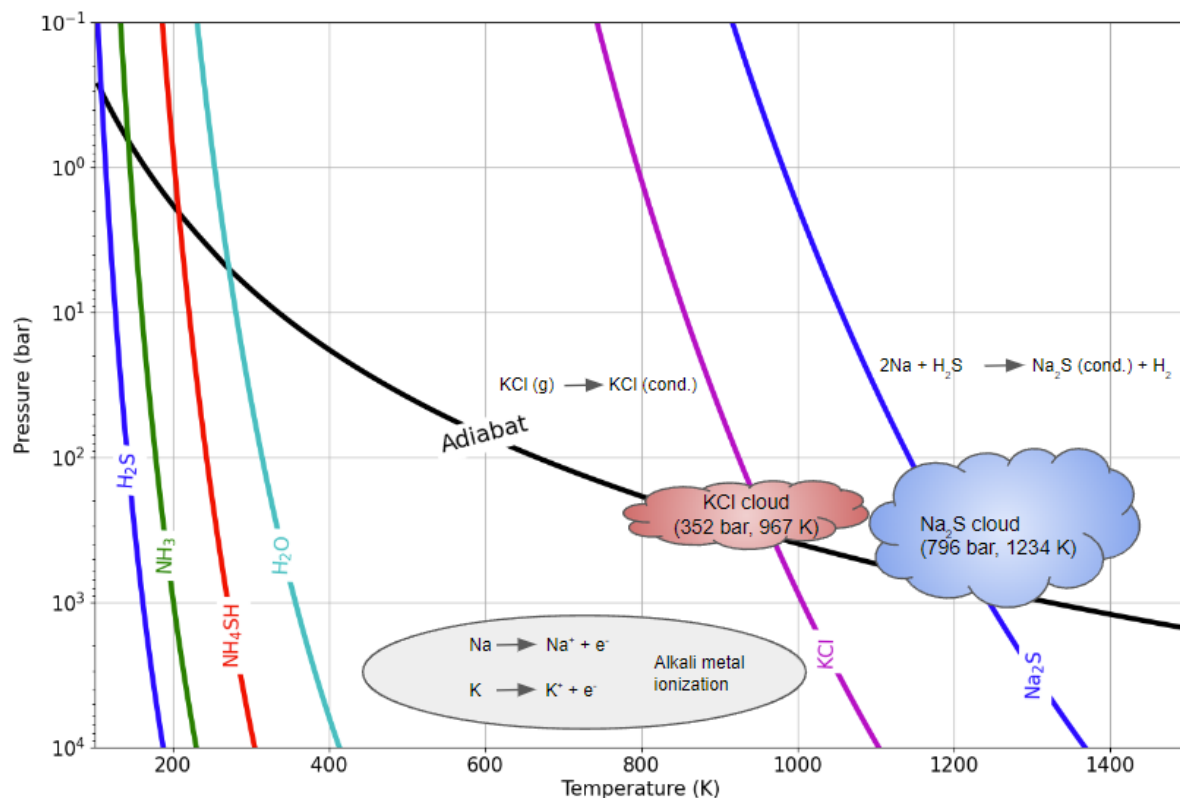


Figure 2. Condensation curves of NH_3 , H_2O , H_2S and alkali metals Na_2S and KCl at 1X solar abundance. Our calculations are based on the equilibrium cloud condensation model [Atreya et al. (1999)], and saturation vapor pressure corresponding to Na_2S and KCl [Visser et al. (2006), Morley et al. (2012)]. The cloud bases are at the levels where the condensation curves cross the adiabat considering $T_{1\text{bar}} = 166.1$ K [Seiff et al. (1998)].

At high pressures 100 bar and beyond, alkali metals would undergo ionization to form cold plasma, and the electrons generated in the process would act as an additional source of opacity at microwave frequencies. The number density of free electrons due to the ionization of alkali metal atoms in the gas phase and is calculated using the Saha ionization [Saha (1920)] (Eq. 2) equation assuming Jupiter’s atmosphere to be in a state of thermal equilibrium. The ionization equation itself assumes a single component gas phase system. Thereby, we add the electron densities from ionization of sodium and potassium to determine total number density of free electrons. Here, N_e is the electron density, N is number density, ϵ is ionization energy, λ is De Broglie wavelength, g_0 and g_1 are statistical weights, k_B is Boltzmann

constant, m_e is mass of the electron and h is Planck's constant.

$$\frac{N_e^2}{N - N_e} = \frac{2}{\lambda^3} \frac{g_1}{g_0} e^{-\epsilon/k_B T} \quad (2)$$

$$\lambda = \sqrt{\frac{h^2}{2\pi m_e k_B T}} \quad (3)$$

The brightness temperatures correspond to electromagnetic radiation traveling from the interior of Jupiter radially outwards through the atmospheric layers. Thus, the transmission through the deep atmosphere is similar to the transmission through a cold plasma medium. The refractive index of microwaves propagating through a cold plasma media can be described by the Appleton- Hartree equation [Helliwell (2014)]. The formulation is applicable to low-temperature plasma medium both in the presence or absence of magnetic fields. At 100-1000 bar pressure levels, the contribution of the magnetic field is insignificant in the Appleton-Hartree formulation [Helliwell (2014)]. Therefore, a simplified version of the Appleton-Hartree equation (Eq. 4) is used to calculate the complex refractive index of the deep atmosphere using the electron number density calculated from the Saha ionization equation. For an unmagnetized cold plasma medium i.e. Jupiter's deep atmosphere, the Appleton- Hartree equation is simplified to:

$$n^2 = 1 - \frac{X}{1 - iZ} \quad (4)$$

$$\alpha = \frac{2\pi}{\lambda_{ch} Q} \quad (5)$$

Here, $X = \frac{\omega_0^2}{\omega^2}$, $Z = \frac{\nu}{\omega}$, ω_0 is electron plasma frequency, ω is the angular frequency of microwave radiation, ω_h is electron gyro frequency, ν is electron- neutral collision frequency, λ_{ch} is the frequency of a given MWR channel, n is the refractive index, α is the extinction coefficient and Q is the quality factor i.e. the ratio of squares of real and imaginary parts of the refractive index.

3.2. Radiative Transfer Modeling

In order to draw a comparison between the MWR observations and theoretical knowledge of Jupiter's atmosphere, a benchmark model for the ideal Jupiter atmosphere is constructed using a moist hydrostatic adiabat following the ideal gas law [Li et al. (2018b), Li et al. (2018a)]. The specific heat of hydrogen is estimated from the mixing ratio of ortho and para hydrogen assuming thermal equilibrium between the ortho and para states. Moreover, the temperature profile of Jupiter's atmosphere is constructed for two cases of reference temperatures: (i) $T = 166.1$ K at the 1-bar pressure level from the Galileo probe [Seiff et al. (1998)] and (ii) $T = 168.8$ K at the 1-bar pressure level based on the reanalysis of the Voyager radio occultation experiment at Jupiter [Gupta et al. (2022)]. Ammonia and water vapor are considered vapors for the moist adiabat and their partial pressure is controlled by the cloud condensation process by forcing the partial pressures to be equal to their saturation vapor pressures. In the deep atmosphere of Jupiter, water and ammonia are not expected to form clouds; however, alkali metals are expected to undergo condensation. Therefore, a similar approach is applied to alkali metals to estimate the concentration of alkali metals present in the gas phase available for the ionization process.

Spectral radiance is proportional to the physical temperature of the atmosphere in the Rayleigh-Jeans limit. For microwave frequencies, we compute the brightness temperature (T_b) from the physical temperature using Eq. (1). The opacity of Jupiter's atmosphere is the sum of opacities from individual sources discussed in the previous section i.e. ammonia, water, free electrons, and collision-induced absorption. The abundances of ammonia and water vapor have been assumed to be 2.7 and 5 times the solar abundance [Li et al. (2020), Li et al. (2017)]. Because there is no a priori information on the alkali metal abundance in Jupiter, Therefore, we compare two cases, one without alkali metals (baseline) and another with alkali metals (treatment) in order to provide a comparison between our current

knowledge of Jupiter and MWR data.

The spatial resolution of MWR data also provides the limb darkening coefficient at six microwave frequencies. Limb darkening (L_d) is defined as the percent change in T_b at a given viewing angle relative to T_b at a position looking vertically down to the planet center i.e. nadir. For our simulations, we compute the limb darkening at a 45-degree angle from the nadir. The MWR channels at 0.6 GHz and 1.2 GHz are chosen to provide a comparison between theory and observations at higher pressures using T_b and L_d as the observables for comparison. The benchmark case of the ideal Jupiter atmosphere is compared with MWR observations as a function of latitude between -40 and 40 degrees planetocentric latitude. Data from higher latitudes are neglected due to the presence of signatures from synchrotron radiation that is inseparable from the atmospheric contribution.

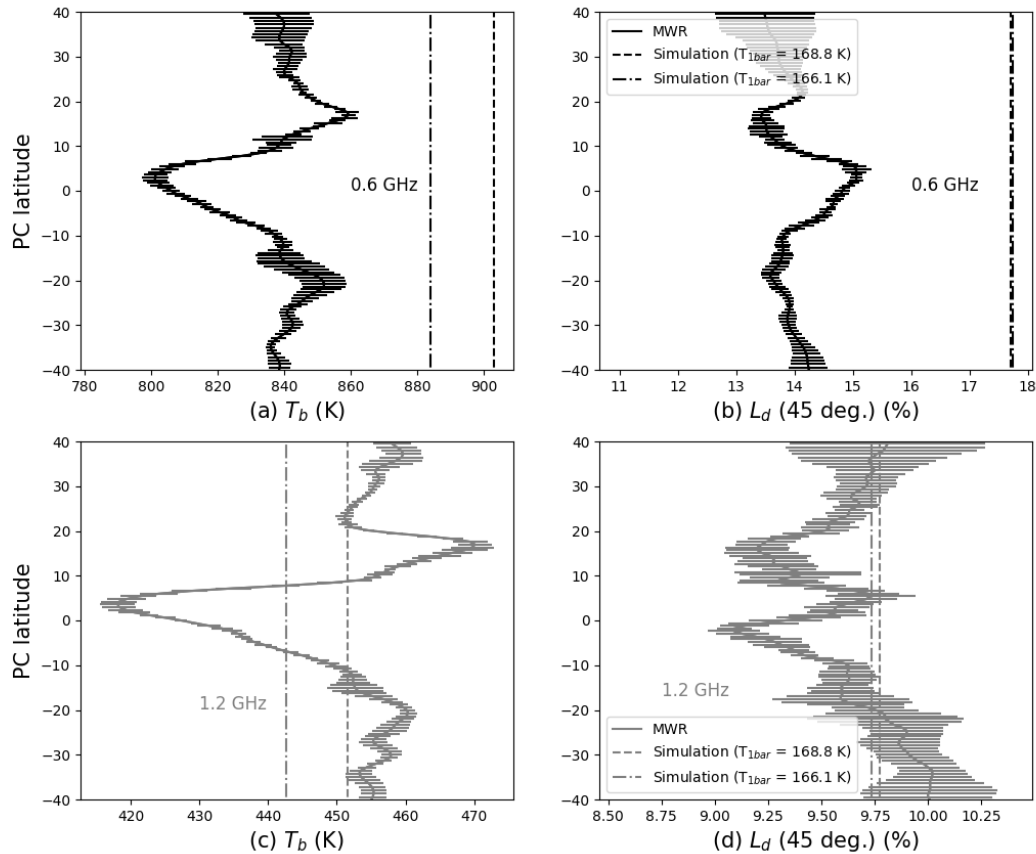


Figure 3. Limb darkening and brightness temperature MWR observations compared with simulation results at 0.6 GHz and 1.2 GHz corresponding to Jovian adiabats at (i) $T_{1bar} = 166.1$ K and (ii) $T_{1bar} = 168.8$ K, (a) T_b vs. latitude at 0.6 GHz, (b) L_d vs. latitude at 0.6 GHz, (c) T_b vs. latitude at 1.2 GHz, (d) L_d vs. latitude at 1.2 GHz.

A latitudinal variation in brightness temperatures is observed at both 0.6 and 1.2 GHz (Figure 3, panels (a) and (c)). The small-scale variations in T_b and L_d in all the panels can be attributed to variations in the atmospheric temperature structure and composition. It is important to note that the baseline case (without alkali metals) corresponds to two different temperature profiles of Jupiter’s atmosphere for two different T_{1bar} . There is an agreement between the baseline case and observations at 1.2 GHz in the equatorial region (panel (c)). On the other hand,

brightness temperatures at 0.6 GHz are lower than the baseline case by 40-60 K at all latitudes (panel (a)) indicating the possibility of an additional source of opacity. Such a source is also supported by a depressed L_d observed by MWR; it is 4 percent less than the L_d magnitude of the ideal Jupiter atmosphere across all latitudes (panel (b)). The mismatch between the baseline and observations at 0.6 GHz is much greater than the uncertainty in measurements and variations in T_b and L_d . Since the brightness temperatures correspond to different pressure regions in the atmosphere, the anomalous observations at 0.6 GHz must be attributed to the presence of an additional opacity source in the deep atmosphere or to a different opacity source that absorbs more effectively at 0.6 GHz than at 1.2 GHz. We test four confounding factors: (1) the distribution of ammonia, (2) the ammonia opacity at temperatures exceeding the range of laboratory measurements, (3) the opacity of water at high temperatures and (4) the contribution of alkali metals. The theoretical brightness temperature and limb darkening at 0.6 GHz and 1.2 GHz is shown in Fig. 3.

The latitudinal distribution of brightness temperatures and limb darkening from the forward model indicates the decrease in limb darkening from the equator to the pole at 0.6 GHz. It is opposite to the variation of limb darkening at 1.2 GHz across the latitudes. This effect could be attributed to the free electrons in the deep atmosphere which could be inferred from the shift in the contribution functions toward higher pressures in presence of alkali metals (Fig. 1). Alkali metals greatly affect the absorption behavior at 0.6 GHz which dominates the effect of gravitation on limb darkening.

3.3. Ammonia, Water and Alkali Metals

Brightness temperature variations with latitude and the spectral inversion of brightness temperatures show a non-uniform distribution of ammonia vapor in Jupiter's atmosphere in the deep atmosphere region [Li et al. (2017), Ingersoll et al. (2017)]. Therefore, the non-uniform distribution of ammonia could contribute to variations in microwave opacity of the deep atmosphere. In order to estimate the effect of ammonia concentration variations, we perturb the ammonia profile in the model and use a scaling factor to vary the magnitude of ammonia vapor concentration in the model as described in Eq. (6).

$$q_{NH_3}(P) = q_{NH_3,0}(P) - (q_{NH_3,0}(P) - q_{NH_3,MWR}(P))s \quad (6)$$

Here, q_{NH_3} is the ammonia mass mixing ratio at a given pressure P , $q_{NH_3,0}(P)$ is the homogeneous ammonia mixing ratio which is set to 2.7 times solar abundance for $NH_3 \sim 360$ ppm [Li et al. (2017)] from the deep atmosphere till the NH_3 vapor saturation point. Above the saturation point, the mixing ratio follows the NH_3 saturation vapor pressure curve. $q_{NH_3,MWR}(P)$ is the mixing ratio retrieved from MWR inversion. We use a scaling factor to vary the ammonia mixing ratio between the homogeneous case to MWR derived profiles. The scaling factor, s ranges from 0 to 1.5 where 0 is the case for homogeneous mixing ratio. Increasing s to 1 will change the ammonia profile to MWR inversion case for equator and mid-latitude regions. We also extend the scaling factor to 1.5, in order to take into account the low ammonia mixing ratio observed at the North Equatorial Belt (NEB) of Jupiter [Li et al. (2017)].

NH_3 opacity measurements are currently not available for high temperatures (550 K-3000 K) corresponding to Jupiter's deep atmosphere and there is a decrease in the magnitude of absorption of NH_3 at high pressures. Thereby, we invoke a scaling factor to the NH_3 absorption coefficient to provide an estimation of the opacity at high temperatures. The mass absorption coefficient of ammonia is estimated by multiplying the temperature-scaling law to the absorption coefficient based on Hanley et al. (2009) (Eq. 7). In this equation, α is the absorption coefficient of NH_3 , h is the opacity factor, T is temperature and T_c is reference temperature equal to 750 K. The NH_3 opacity models show that the absorption coefficient peaks at 750 K and decreases at temperatures beyond 750 K. In the simulations, the scaling factor is multiplied to the NH_3 opacity at temperatures higher than T_c . The power law index (h) is varied from 1 to 5 keeping the ammonia concentration constant, i.e., 2.7 times solar abundance. We also keep the water vapor constant at 5 times solar abundance as the laboratory measurements demonstrate that water vapor absorption does not show a significant increase with pressure and can be said to be relatively transparent when compared to the previous model of microwave absorption [Steffes et al. (2023)].

$$\alpha(NH_3) \sim \left(\frac{T_c}{T}\right)^h \quad (7)$$

Changing the ammonia profile and introducing the additional temperature-dependent scaling factor produce brightness temperature and limb darkening divergent from MWR data at 0.6 GHz as shown in Figure 4a. The difference between T_b from the model and observations is in the range of 50-200 K at 0.6 GHz. Reducing the ammonia concentration causes a monotonic increase in T_b and a decrease in L_d . Further, reducing the ammonia opacity shows a similar trend in T_b , while a saturation in L_d is expected at a power law factor of 5. Changing the ammonia profile and ammonia opacity has a similar effect on T_b and L_d at 1.2 GHz. However, overall, the variation in the MWR observations at 1.2 GHz can be explained by these two factors and does not require the inclusion of alkali metals. The 1.2 GHz observations correspond to ~ 20 bar (Fig. 1), much above the cloud base of alkali metals and at relatively lower pressure levels. Therefore, the contribution of free electrons to opacity is expected to be less due to lower temperatures, and the opacity contribution of ammonia vapor dominates at 1.2 GHz. However, a comparison of MWR observations at both frequencies clearly implies that the variation in ammonia vapor opacity cannot solely explain the anomalous observations at the 0.6 GHz channel.//

Fig. 4c, 4d examines the overall effect of alkali metals and ammonia vapor on the T_b and L_d at 0.6 GHz and 1.2 GHz. We vary the alkali metal metallicities in a range from 0 to -7 (solar abundance of Na and K according to [Asplund et al. \(2009\)](#)) for each condition of NH_3 profile scaling and NH_3 opacity scaling. The volume mixing ratio of Na and K corresponding to abundance in solar photosphere [[Asplund et al. \(2009\)](#)] are 3.46×10^{-6} ($[Na/H] = -5.76$) and 2.14×10^{-7} ($[K/H] = -6.97$), respectively. Therefore, we simulate a wide range of ammonia opacity conditions for a given alkali metal abundance (colored dots). Both NH_3 profile and opacity scaling cause a change in T_b and L_d , which is shown by the annotation in the figure. The variation in T_b and L_d is similar to the pattern in Fig. 4a. NH_3 profile scaling causes a decrease in L_d , while the scaling in NH_3 vapor opacity causes L_d to increase at 0.6 GHz. For each case of metallicity, we then perform a scaling in ammonia vapor and ammonia opacity as described previously in this section. This provides us with a matrix of T_b and L_d to take into account all possible sources of opacity, i.e., collision-induced absorption, ammonia, water vapor, and free electrons from alkali metals. The free electron opacity is calculated from the Hartree-Appleton equation explained in the previous section.

When we compare the new model result with MWR observations (Fig. 4b), we observe that model matches with observations at 0.6 GHz for free electrons corresponding to alkali metal metallicities in the range of -2 to -5 (chocolate colored patches), i.e. 10^{-2} to 10^{-5} times the solar abundance. There is an agreement between the model and observations at 1.2 GHz for the same range of metallicities. The addition of free electrons from alkali metals dominates the effect of gravity (Fig. 5) and we expect the limb darkening to decrease from equator to the poles assuming uniform mixing ratio of water and ammonia vapor. It serves as a baseline to understand the sole effect of free electrons on latitudinal variation of microwave radiation from Jupiter's deep atmosphere.

4. DISCUSSIONS

We infer metallicity of the alkali metals in Jupiter to be much lower than the solar value. A possible indication of low metallicity of the alkali metals in a hot Jupiter exoplanet was first proposed by [Demory et al. \(2011\)](#) as one plausible explanation for the high albedo of Kepler-7b. They derived an alkali metal abundance 10-100 times lower than the solar value. Since then the abundance of alkali metals has been derived for several other giant exoplanets, with abundances ranging from ~ 100 times below solar to ~ 100 times above solar, although the uncertainties are large. Recent observations of two hot Jupiters or Saturns with clear or mostly clear atmospheres were made. The alkali metal abundance for one such hot Jupiter (HAT-P-1b) is found to be sub-solar [[Chen et al. \(2022\)](#)], while it was found to be solar to greatly super-solar for the other (WASP-96b)[[Nikolov et al. \(2022\)](#)]. Considering the relatively small sample size of hot Jupiters with clear atmospheres, it is premature to make a meaningful comparison between their alkali metal metallicity and the metallicity in Jupiter presented in this paper. On the other hand, it is instructive to compare the abundance of alkali metals in Jupiter from this work with the abundance of the other heavy elements. While the opacity contribution from alkali metals suggest that Na and K are strongly depleted relative to solar at the level probed by MWR at 0.6 GHz, all other heavy elements are enriched by a factor of approximately three to five; while nitrogen is highly variable but enriched, and the water abundance remains uncertain [[Atreya et al. \(2019\)](#)], Li

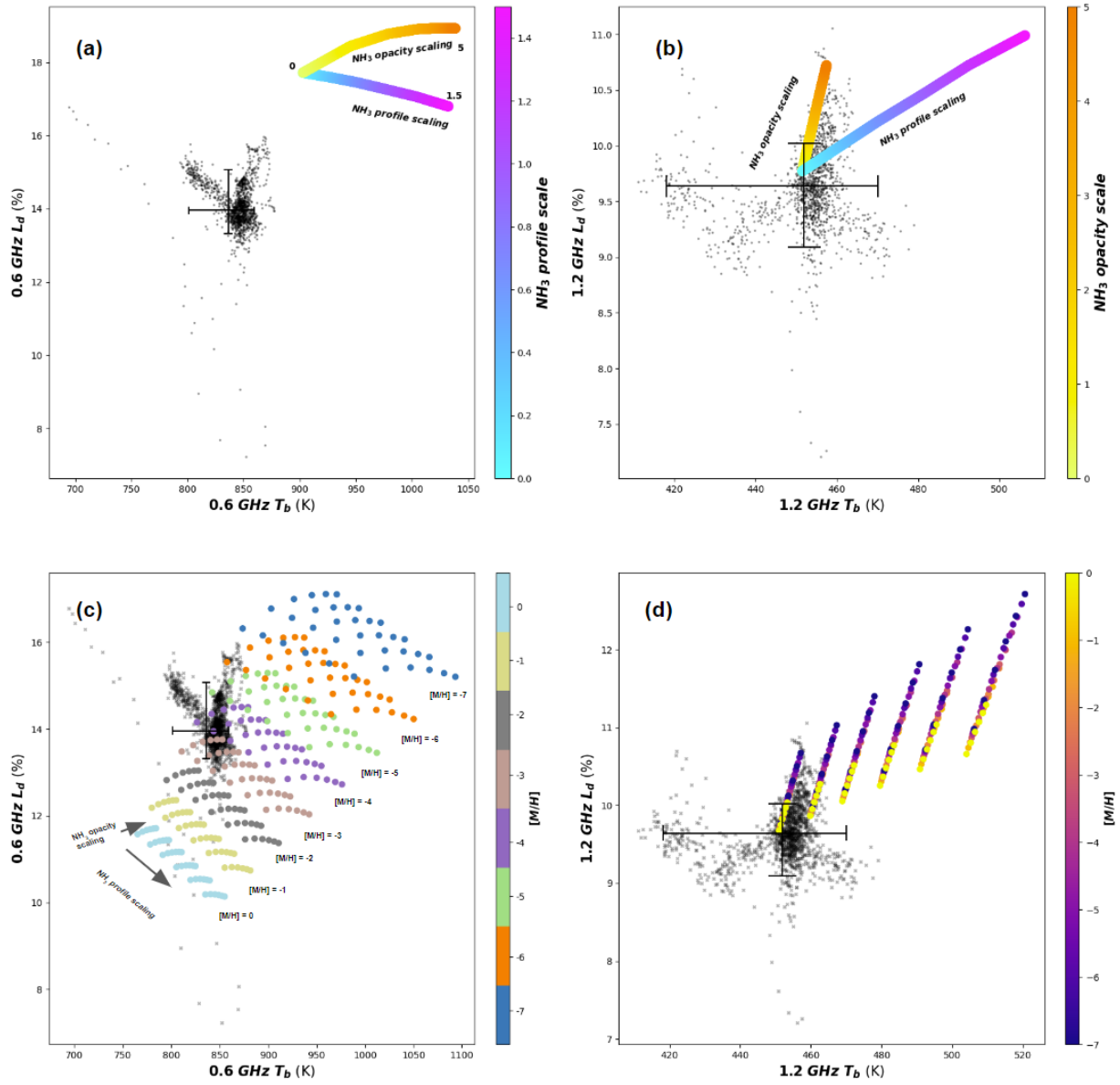


Figure 4. Comparison is drawn between the Juno MWR observations and the results of the radiative transfer model for T_b and L_d at 0.6 GHz and 1.2 GHz, keeping the water abundance constant ~ 5 times solar abundance. (a, b) Jupiter’s atmosphere in the absence of alkali metals with only variations in the NH_3 vapor profile and the NH_3 opacity, (c, d) Jupiter’s atmosphere in the presence of alkali metals with variations in the NH_3 vapor profile and the NH_3 opacity. The NH_3 profile of Jupiter’s atmosphere is varied using a scale from 0 to 1.5 to take into account the contribution of non-uniform distribution of NH_3 vapor observed by MWR [Li et al. (2017)]. NH_3 opacity at temperatures above 750 K undergoes power law scaling as a function of atmospheric temperature (Eq. 7). In the absence of alkali metals, the changes in NH_3 vapor profile and the scaling in NH_3 vapor opacity deviate significantly from Juno MWR observations at 0.6 GHz. However, in the presence of alkali metals of low metallicity, i.e., in the range of -2 to -5, there is an agreement between model results and MWR observations. Observations at 1.2 GHz can be explained by variations in the NH_3 vapor profile and the NH_3 opacity independent of opacity contributions from alkali metals.

et al. (2020), Li et al. (2017), Mahaffy et al. (2000)]. The comparison to other heavy metal measurements from the Galileo probe corresponds to much lower pressures i.e. < 22 bars. The estimation of alkali metal metallicity from MWR implies lower metallicity at much higher pressures. The results (Fig. 4b) provide an important constraint on alkali metal abundance at pressures sensitive to 0.6 GHz channel. A $[\text{M}/\text{H}] = -1$ for alkali metals provides too much opacity while too little abundance or absence of alkali metals does not provide sufficient opacity to match the MWR

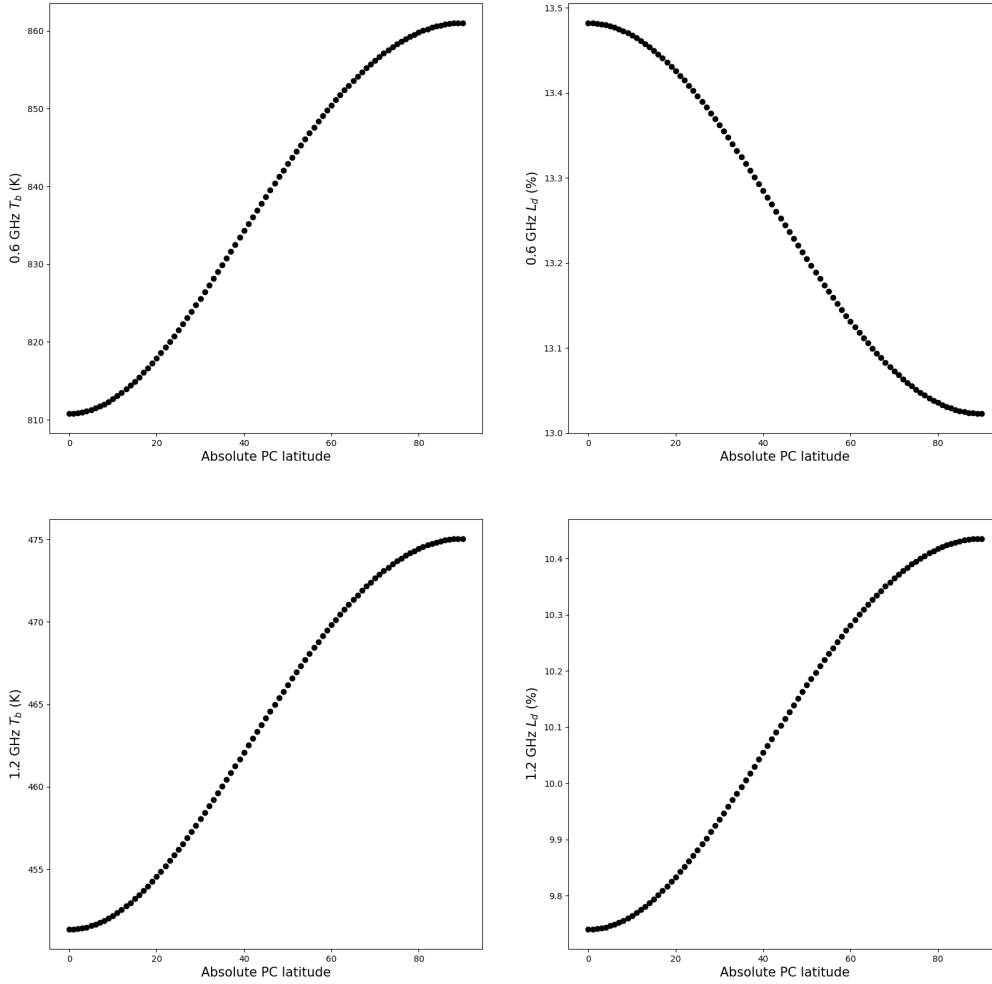


Figure 5. Latitudinal variation of brightness temperature and limb darkening of Jupiter’s atmosphere at 0.6 GHz and 1.2 GHz at $[M/H] = -3$

observations at 0.6 GHz.

The low abundance of alkali metals indicated by MWR observations could be attributed to any of the following scenarios. (i) Initially enriched alkali metals, consistent with the other heavy elements in the atmosphere, are depleted by chemical reactions with other constituents deep in the atmosphere, resulting in a low abundance of Na and K at ~ 1 kilobar level sufficient to provide the free electrons to explain the MWR data at 0.6 GHz. Fegley and Lodders [Fegley Jr & Lodders (1994)] predict, for example, the formation of gas-phase species of Na and K in the atmosphere i.e. NaCl, NaOH, and KOH. Should there be chemical mechanisms that could selectively deplete K in the atmosphere, leaving Na to be the most significant contributor to free electrons in the deep atmosphere, the metallicity of Na would be expected to be in the range of 0 to -2 i.e. solar to highly sub-solar abundance (Appendix B). (ii) Unconventional planet formation processes, whereby Jupiter did not accrete a solar complement of alkali metals, or that the alkali metals are not well mixed at greater depths. If the depletion of alkali metals at ~ 1 kbar inferred in this paper is

representative of their bulk abundance, it could be indicative of the depletion of all rock-forming elements, with significant implications for the formation and evolution of Jupiter. Our conclusion of depletion is based on the data of the 0.6 GHz channel, whose weighting function peaks at 1 kilobar level with the inclusion of alkali metals. Thus, we are confident about the result only at this level. Alkali metals could well be more abundant deeper in the atmosphere and they could have been depleted by some as yet unknown mechanism before reaching the 1 kilobar level though the degree of depletion would have to be huge. Barshay & Lewis (1978) considered one such possibility, where silicates were found to be a way of sequestration of gas phase alkali metals. However, a later study by Fegley Jr & Lodders (1994) found it to be an ineffective mechanism. Further modeling and laboratory studies are needed to cover the full parameter space of combined thermochemistry of alkali metal and rock cloud forming species corresponding to the very high temperature and high pressure conditions of the deep atmosphere of Jupiter, together with any dynamical effects, before drawing any firm conclusions about depletion of alkali metals in bulk Jupiter below the level to which the MWR data of this paper are sensitive.

The new constraints on the abundance of alkalis are linked to their low ionisation potential, and the fact that the electrons that they provide directly affect opacities at 0.6 and 1.2 GHz (see Eq. 4). But when present, they are strong absorbers at visible wavelengths (e.g., Burrows et al. (2000)) and therefore directly affect the planetary radiative flux. The low abundances that we derive imply that a radiative zone may be present in Jupiter [Guillot et al. (1994), Guillot et al. (2004)]. Interestingly, this could explain at the same time the relatively low abundance of CO observed in Jupiter’s atmosphere compared to expectations for a fully convective deep atmosphere [Cavalié et al. (2023)].

5. SOFTWARE AND THIRD PARTY DATA REPOSITORY CITATIONS

The software for the radiative transfer package will be available at zenodo archive (<https://doi.org/10.5281/zenodo.7893914>) and the MWR data used in this work, and associated files for data visualization are available at archive (<https://doi.org/10.5281/zenodo.7893817>). They can be made available upon request

Software: High-performance Atmospheric Radiation Package (HARP) [Li et al. (2018b), Bhattacharya et al. (2023)]

APPENDIX

A. APPENDIX A: ELECTRON DENSITY AND CONDUCTIVITY

The electron density of Jupiter’s atmosphere is governed by two fundamental processes: (i) condensation of alkali metal condensates i.e. Na_2S and KCl , and (ii) ionization of alkali metals in thermal equilibrium. Fig. 2 shows the pressure levels corresponding to the cloud base of Na_2S and KCl based on their saturation vapor pressures. Cloud condensation reduces the amount of alkali metals available in gas phase that act as a source of free electrons, and restricts the abundance of Na and K corresponding to their respective saturation vapor pressure. In the cloud region, electron density is controlled by saturation vapor pressure of alkali metals whereas below the cloud base, electron densities are governed by metallicity of alkali metals. Thereby, it is evident that condensation controls the electron density and thereby, conductivity at low pressure levels. Condensation limited ionization is observed at low pressure (below 1 kbar) irrespective of the alkali metal abundance as the electron density lines converge (Fig. A.1 (a)). Fig. A.1 (a) and (b) show the presence of a kink in electron density and their respective conductivity at the cloud base corresponding to different alkali metal abundances. However, condensation does not play a significant role in governing the electron densities at ~ 1 kbar pressure level corresponding to the global maxima in the weighting function at 0.6 GHz (Figure 1).

The electron density of the deep atmosphere is much lower than in the case of alkali metals at solar abundance. It is the true representation of the electron density of the deep atmosphere. At greater pressures, hydrogen behaves as a semiconductor and becomes the major contributor to the electron density [Liu et al. (2008)]. The electrical conductivity of the atmosphere is calculated using Drude’s equation. It provides an estimate of the conductivity due to the free electrons provided by alkali metal ionization.

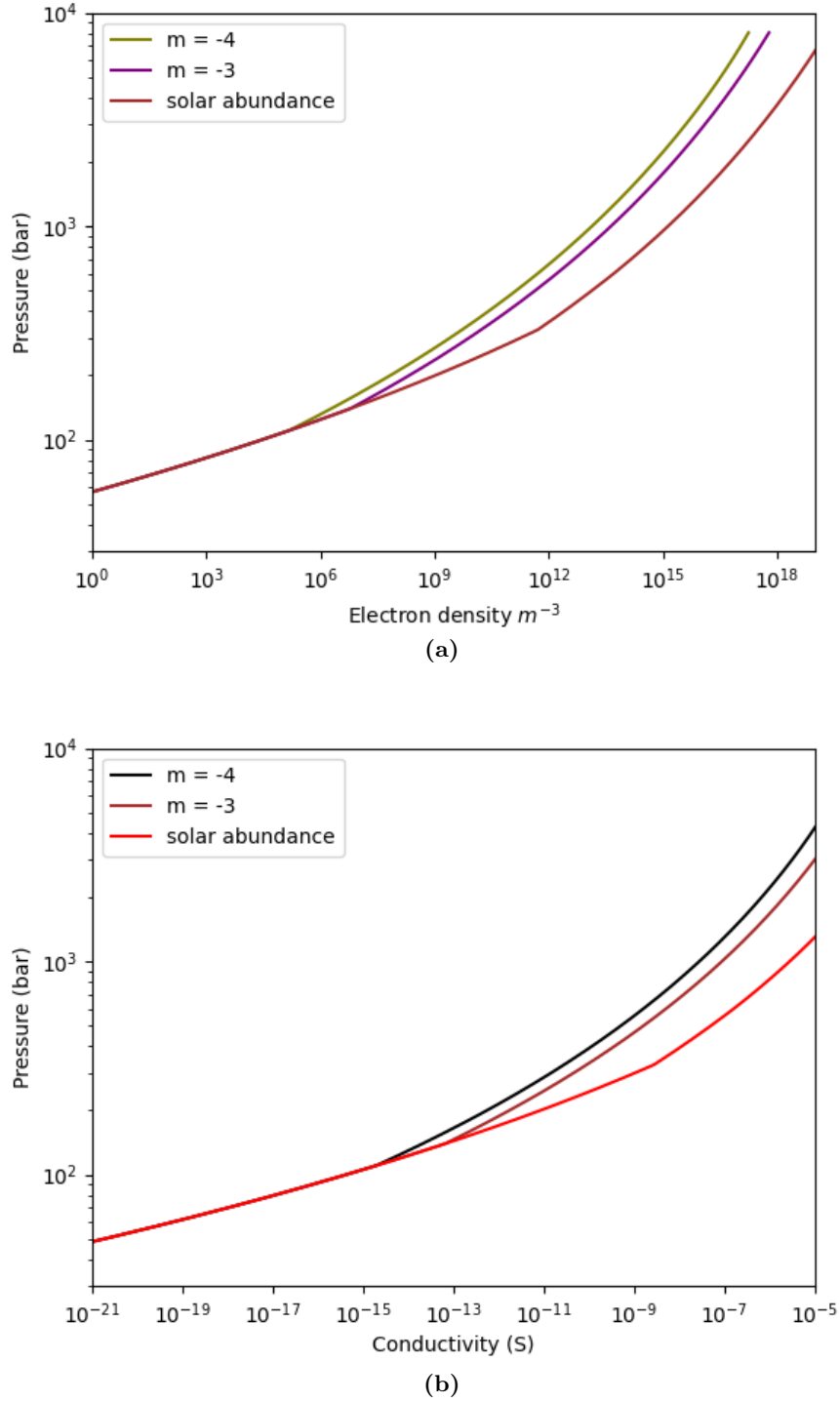


Figure A.1. (a) Electron density of Jupiter's deep atmosphere at the solar abundance and $[M/H] = -3$ and -4 , (b) electrical conductivity of Jupiter's deep atmosphere at the solar abundance and $[M/H] = -3$ and -4 .

B. APPENDIX B: SELECTIVE DEPLETION OF ALKALI METALS

Even though Na_2S has a deeper condensation level compared to KCl , the cloud condensation is governed by atmospheric temperature, and does not reflect the chemical reactivity of alkali metals. K is more electropositive than Na

and thereby, is expected to be more reactive as compared to Na. Therefore, it is possible that there can be a chemical mechanism that could selectively deplete K into other compounds, leaving Na as the only source of free electrons in Jupiter. Under such conditions, we find that Na metallicity should be in the range of 0 to -3 to match the MWR observations. The increase in alkali metal metallicities can be attributed to two factors: (i) low ionization energy of K, and (ii) Na_2S condenses much below KCl (Figure 2). Thereby, a larger amount of Na is required to produce enough free electrons to match the MWR brightness temperatures and limb darkening.

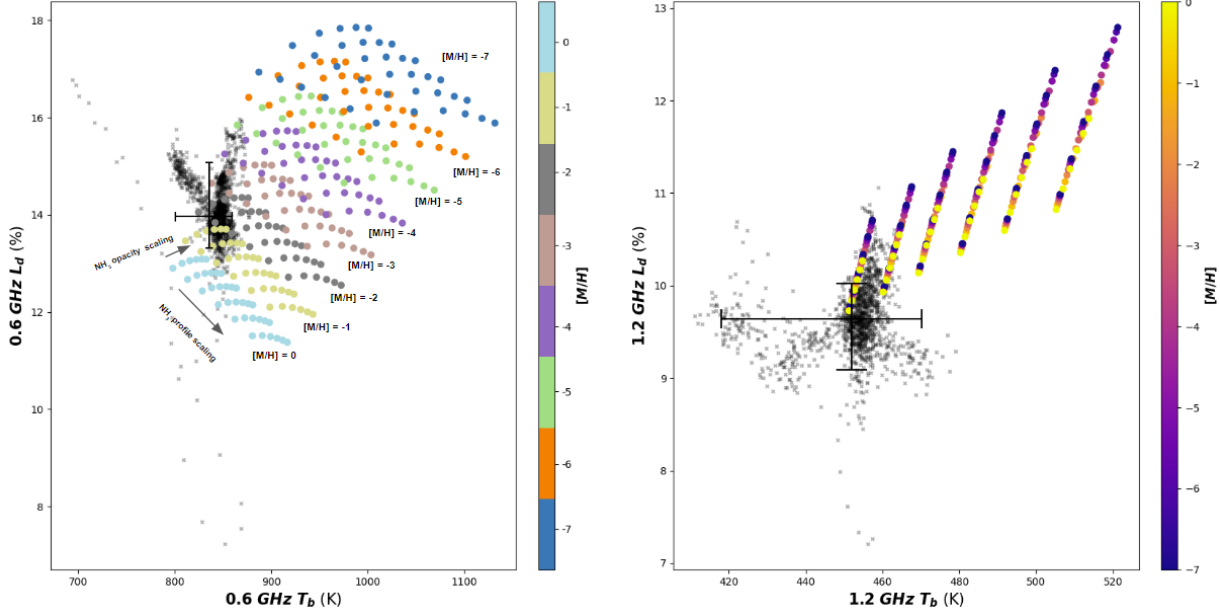


Figure B.1. Limb darkening and brightness temperature comparison of MWR observations and forward model results at 600 MHz and 1.2 GHz for metallicities ranging from 0 to -7 at different ammonia vapor concentration profiles and opacities. It showcases the sole effect of free electrons due to the ionization of Na, without considering any contribution from K.

The elimination of K from the atmosphere highlights the role of the elemental abundance of Na required to match the MWR observations. The results of the forward model in Fig. B.1 indicate the possible solutions of Na metallicity under different conditions of ammonia vapor concentration profiles and microwave opacities. It is observed that the range of Na metallicity is expected to be from 0 to -3 i.e. solar abundance to highly sub-solar abundance. Thus, metallicity of Na required is expected to be higher than those considering both Na and K to be sources of free electrons.

C. APPENDIX C: JOVIAN ADIABATS AND COMPARISON OF MWR WITH HIGH TEMPERATURE ADIABAT

Fig. 2 shows that brightness temperatures at 600 MHz from two adiabats differ by approximately 15 K. The relative weighting function for the adiabats is that of the ideal Jupiter’s atmosphere without the inclusion of opacity due to free electrons from alkali metals. It shows a peak at ~ 100 bar. From the difference in physical temperature of the atmosphere of the two adiabats, it is seen that the difference reaches ~ 10 -15 K at 100 bar level (Fig. C.1). The weighting function at 600 MHz also extends below 100 bar which could explain the difference in brightness temperatures. An interesting observation is that the difference in adiabat temperatures increases with increase in atmospheric pressure. This increase can be attributed to the temperature dependent specific heat of the atmospheric constituents.

The interior models of Jupiter generally use a high temperature in the range of 170-180 K at the outer boundary (1 bar pressure level) [Gupta et al. (2022), Miguel et al. (2022)]. These temperatures are about 10-15 K higher than the measurements from the Galileo probe (166.1 K)[Seiff et al. (1998)] and Voyager radio occultation reanalysis (168.8

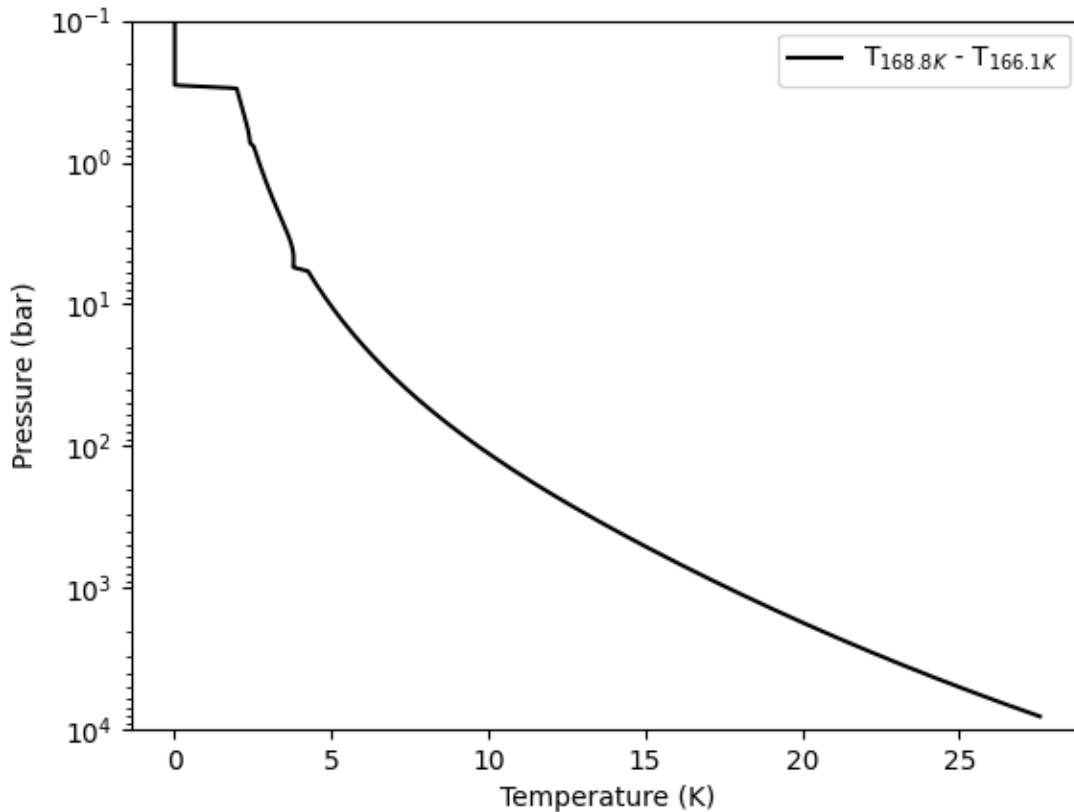


Figure C.1. Pressure v. temperature difference in temperatures of Jovian adiabats constructed using $T_{1bar} = 168.8$ K and $T_{1bar} = 166.1$ K

K)[Gupta et al. (2022)]. A simulation of brightness temperatures and limb darkening at 0.6 GHz and 1.2 GHz is carried out for all cases of alkali metal metallicities, ammonia concentration and opacity variation assuming $T_{1bar} = 175$ K. It can be clearly seen in Fig. C.2 that high temperature at 1 bar doesn't match with entire range of MWR observations for both the frequencies. Some alternate possibilities could be the presence of a non-adiabatic gradient or a radiative layer in Jupiter's deep atmosphere that can possibly account for a higher temperature at 1 bar level. However, the mismatch with MWR at 1.2 GHz poses a serious question on the assumption. The current measurements of temperature at 1 bar level are from limited radio occultation experiments. There is a need for radio science experiments from equator to the poles, in order to estimate the true variability in temperatures at 1 bar.

REFERENCES

- Asplund, M., Grevesse, N., Sauval, A. J., & Scott, P. 2009, Annual review of astronomy and astrophysics, 47, 481
- Atreya, S., Wong, M., Owen, T., et al. 1999, Planetary and Space Science, 47, 1243
- Atreya, S. K., Crida, A., Guillot, T., et al. 2019, The origin and evolution of Saturn, with exoplanet perspective, in "Saturn in the 21st Century", (Eds. Baines K. H. et al.), pp. 5-43, Cambridge University Press Cambridge, UK
- Bagenal, F., Dowling, T. E., & McKinnon, W. B. 2007, Jupiter: the planet, satellites and magnetosphere, Vol. 1 (Cambridge University Press)
- Barshay, S. S., & Lewis, J. S. 1978, Icarus, 33, 593
- Bellotti, A., Steffes, P. G., & Chinsomboon, G. 2016, Icarus, 280, 255
- Bhattacharya, A., Li, C., Atreya, S. K., et al. 2023, HARP Radiation Package for Planetary Atmospheres, Zenodo, doi: [10.5281/zenodo.7893914](https://doi.org/10.5281/zenodo.7893914)

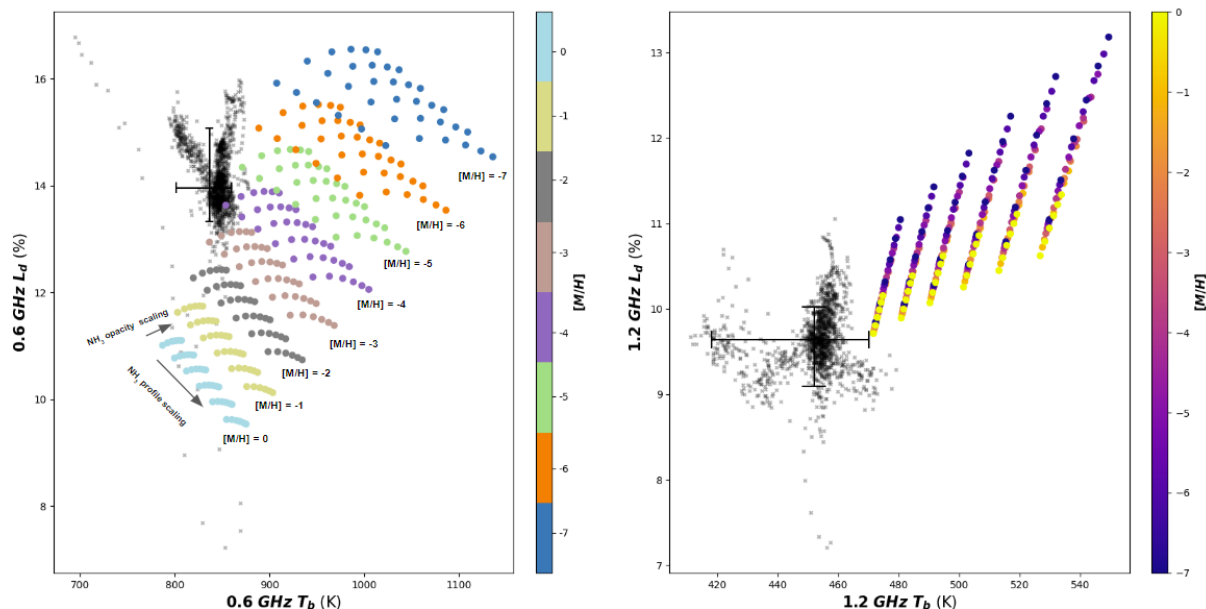


Figure C.2. Limb darkening and brightness temperature comparison of MWR observations and forward model results at 600 MHz and 1.2 GHz for metallicities ranging from 0 to -7 at different ammonia vapor concentration profiles and opacities considering $T_{1bar} = 175$ K

- Bolton, S. J., Adriani, A., Adumitroaie, V., et al. 2017, *Science*, 356, 821
- Burrows, A., Marley, M., & Sharp, C. 2000, *The Astrophysical Journal*, 531, 438
- Cavali , T., Lunine, J., & Mousis, O. 2023, *Nature Astronomy*, 1
- Chen, G., Wang, H., van Boekel, R., & Pall , E. 2022, *The Astronomical Journal*, 164, 173
- Chen, G., Pall , E., Welbanks, L., et al. 2018, *Astronomy & Astrophysics*, 616, A145
- de Pater, I., & Dunn, D. E. 2003, *Icarus*, 163, 449
- de Pater, I., Sault, R., Wong, M. H., et al. 2019, *Icarus*, 322, 168
- Demory, B.-O., Seager, S., Madhusudhan, N., et al. 2011, *The Astrophysical Journal Letters*, 735, L12
- Devaraj, K., Steffes, P. G., & Duong, D. 2014, *Icarus*, 241, 165
- Fegley Jr, B., & Lodders, K. 1994, *Icarus*, 110, 117
- Guillot, T., Chabrier, G., Morel, P., & Gautier, D. 1994, *Icarus*, 112, 354
- Guillot, T., Stevenson, D. J., Hubbard, W. B., & Saumon, D. 2004, *The interior of Jupiter*, in "Jupiter: The planet, satellites and magnetosphere", (Eds. Bagenal F. et al.), Cambridge University Press New York
- Gupta, P., Atreya, S. K., Steffes, P. G., et al. 2022, *The Planetary Science Journal*, 3, 159
- Hanley, T. R., Steffes, P. G., & Karpowicz, B. M. 2009, *Icarus*, 202, 316
- Heays, A., Bosman, AD, v., & Van Dishoeck, E. 2017, *Astronomy & Astrophysics*, 602, A105
- Helliwell, R. A. 2014, *Whistlers and related ionospheric phenomena* (Courier Corporation)
- Ingersoll, A. P., Adumitroaie, V., Allison, M. D., et al. 2017, *Geophysical Research Letters*, 44, 7676
- Janssen, M., Oswald, J., Brown, S., et al. 2017, *Space Science Reviews*, 213, 139
- Karpowicz, B. M., & Steffes, P. G. 2011, *Icarus*, 212, 210
- Levin, S. M., Bolton, S. J., Gulikis, S. L., et al. 2001, *Geophysical research letters*, 28, 903
- Li, C., Ingersoll, A. P., & Oyafuso, F. 2018a, *Journal of the Atmospheric Sciences*, 75, 1063
- Li, C., Le, T., Zhang, X., & Yung, Y. L. 2018b, *Journal of Quantitative Spectroscopy and Radiative Transfer*, 217, 353
- Li, C., Ingersoll, A., Janssen, M., et al. 2017, *Geophysical Research Letters*, 44, 5317
- Li, C., Ingersoll, A., Bolton, S., et al. 2020, *Nature Astronomy*, 4, 609
- Liu, J., Goldreich, P. M., & Stevenson, D. J. 2008, *Icarus*, 196, 653, doi: <https://doi.org/10.1016/j.icarus.2007.11.036>
- Mahaffy, P., Niemann, H., Alpert, A., et al. 2000, *Journal of Geophysical Research: Planets*, 105, 15061

- Miguel, Y., Bazot, M., Guillot, T., et al. 2022, *Astronomy and Astrophysics-A&A*, 662
- Morley, C. V., Fortney, J. J., Marley, M. S., et al. 2012, *The Astrophysical Journal*, 756, 172
- Nikolov, N. K., Sing, D. K., Spake, J. J., et al. 2022, *Monthly Notices of the Royal Astronomical Society*, 515, 3037
- Saha, M. N. 1920, *The London, Edinburgh, and Dublin Philosophical Magazine and Journal of Science*, 40, 472
- Santos-Costa, D., Adumitroaie, V., Ingersoll, A., et al. 2017, *Geophysical research letters*, 44, 8676
- Seiff, A., Kirk, D. B., Knight, T. C., et al. 1998, *Journal of Geophysical Research: Planets*, 103, 22857
- Steffes, P. G., Bellotti, A., Cembellin, P., Levin, S. M., & Bolton, S. J. 2023, *The Planetary Science Journal*
- Steffes, P. G., Hanley, T. R., Karpowicz, B. M., et al. 2017, *Space Science Reviews*, 213, 187
- Visscher, C., Lodders, K., & Fegley Jr, B. 2006, *The Astrophysical Journal*, 648, 1181
- Weidenschilling, S., & Lewis, J. 1973, *Icarus*, 20, 465
- Welbanks, L., Madhusudhan, N., Allard, N. F., et al. 2019, *The Astrophysical Journal*, 887, L20
- Wong, M. H., Mahaffy, P. R., Atreya, S. K., Niemann, H. B., & Owen, T. C. 2004, *Icarus*, 171, 153